Estimating Photometric Redshifts Using Template-Based and Empirical-Based Methods on Faint Galaxies Detected by a 0.4m Diameter Telescope.

Physics Department, University of California, Santa Barbara

Santa Barbara, CA 93106, USA

(Dated: June 14, 2023)

Abstract

Using template-based and empirical based methods, we conduct a photometric redshift survey for six galaxies and compare the effectiveness of the two methods. We measured the flux from four different galaxies on a 0.4m SBIG STL 6303 telescope. From the images, we calculated the flux and hence asinh magnitude from the galaxies. These values are plugged into two different programs, HyperZ and k-nearest neighbors, to estimate a redshift value. We compare the effectiveness of using two different methods for finding the photometric redshift. For six galaxies, our resulting percent differences from the accepted redshift for each using HyperZ for were 1 2900%, 353%, 801%, 274%, 42.5%, 6038%, and 18500%. The percent differences using the Nearest Neighbor method were 9430%, 439%, 781%, 174%, 10.6%, 43.2% and 85.9%. In conclusion, photometric redshift estimation with a smaller aperture telescope arises a variety of difficulties, and our current methods are significantly inaccurate for galaxies at very low redshifts.

I. INTRODUCTION

A galaxy's redshift helps scientists gauge the relative distance between the galaxy and our Milky Way. Redshifts are significant because they define the basis of the Hubble constant, a fundamental concept that led today's scientists to explore the expanding universe, the cosmic horizon, and the Big Bang.

The basic equation for redshift is given by the formula [1]:

$$z = \frac{\lambda_{obs} - \lambda_{em}}{\lambda_{em}} \tag{1}$$

where λ_{obs} is the observed wavelength ,and λ_{em} emitted wavelength.

There are two major techniques used to measure redshift: spectroscopy and photometry. Spectroscopy analyzes the electromagnetic spectrum of a celestial object and reveals the object's temperature, chemical composition, and motion. By comparing the emitted spectra and the observed spectra of the object, the redshift is found by finding the shift of observed spectra [2]. Photometry measures the brightness of celestial objects to determine their physical properties. Spectroscopic redshift measurements are more accurate and precise in comparison to photometric redshift measurements because spectroscopy measures the exact shift in wavelength. Photometric redshifts measurements are found by using the object's brightness and color and comparing it to known data. From this comparison, an estimate of the redshift can be made albeit the value is more affected by uncertainties [3]. A visual comparison between spectroscopic and photometric measurements is illustrated in Figure 1.

While spectroscopy yields more accurate values, photometry provides an efficient method to find redshifts of a larger number of objects than spectroscopy. The redshift of hundreds of objects can be estimated in a single photometric survey in comparison to a spectroscopy survey [1]. As such, photometry has become a vital technique to quickly estimate the redshifts of many celestial bodies.

The purpose of this paper is to explore the use of photometry to find redshift values us-

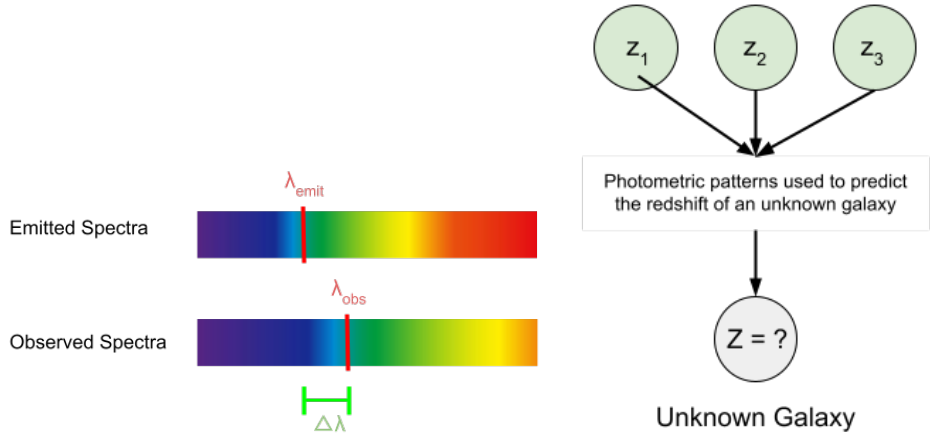

FIG. 1: Comparison between spectroscopic redshift and photometric redshift. Spectroscopy (left) can locate specific wavelength shifts. Photometry (right) estimates redshifts with known data.

ing a smaller, weaker telescope. Two estimation approaches are implemented in this paper: template-based approach and empirical-based approach. Template-Based approach uses spectral templates called spectral energy distributions (SED) and synthesizes photometric magnitudes at various redshifts. A redshift estimation is calculated by finding the least difference between the experimental magnitude and the magnitude of different templates. The empirical-based approach relies on the similarity between an object's photometric data and the patterns to estimate a redshift value. The similarity is expressed in a metric space called the distance metric [4]. This paper uses a 3 dimensional vector space: r-band magnitude, g-r color index, and r-i color index.

The database used for the empirical-approach is the Sloan Digital Sky Survey (SDSS), specifically the most recent data release, DR 17. The SDSS database is chosen due to the advantageous search engine. The database provides broad-band magnitudes and redshifts of objects in bulk. In addition, the redshifts of all the galaxies are photometrically and spectroscopically cross checked [5].

The standard magnitude convention utilizes a bright star, Vega, as magnitude zero. In astronomical magnitude scale, zero stands for the brightest magnitude. An increase in mag-

Galaxy Letter	Galaxy Name	Accepted Redshift
A	NGC 4594 (Sombrero Galaxy)	0.003416 ± 0.000017
B	2MASX J12275231-1120370	0.08504 ± 0.00015
C	6dFGS gJ124555.9-424016	0.04768 ± 0.00015
D	2dFGRS TGN132Z253	0.11333 ± 0.00003
E	M101 (Pinwheel Galaxy)	0.000811 ± 0.000016
F	NGC 4151	0.003262 ± 0.000067

TABLE I: Table will all galaxies referenced in this paper with their accepted values of redshift. Images of galaxies A-D were obtained using the LCO telescope system and E,F were taken from SIMBAD [7] for testing purposes.

nitude value decreases the object's brightness. This paper implements an inverse hyperbolic sine magnitude scale system (asinh). Asinh magnitudes have a lower signal-to-noise ratio. This allows for more accurate magnitude measurements of fainter objects. Researchers often use the asinh scale due to its linearity, allowing for efficient data analysis and for reduced systematic errors [6]. Explanations on Asinh magnitude calculations are further described in Section 2.2.b.

This paper finds an experimental redshift of four different galaxies using a 0.4 meter SBIG STL-6303 telescope from Las Cumbres Observatory (LCO). The four galaxies are listed as Galaxy A, B, C, and D in Table I. Galaxies E and F are test galaxies used to analyze the accuracy of the template-based and empirical-based redshift calculations.

Our approach is significant as photometric research quicken data collection for thousands of celestial objects in many databases. Our goal is to conduct photometric redshift estimation on a small diameter telescope and to understand the current photometric redshift programs for smaller redshift values.

II. METHODS

The basic structure of the methods is as follows. In section 2(A) and 2(B), the observational methods and data extrapolation process is described respectively. Section 2(C) explains which magnitude scales are used and how magnitudes are calculated. Finally, Section 2(D) and Section 2(E) explains how the template-based and empirical-based approach estimates a redshift value. The experimental procedure follows in this respective order. A simple diagram illustrating the procedure is depicted in Figure 2.

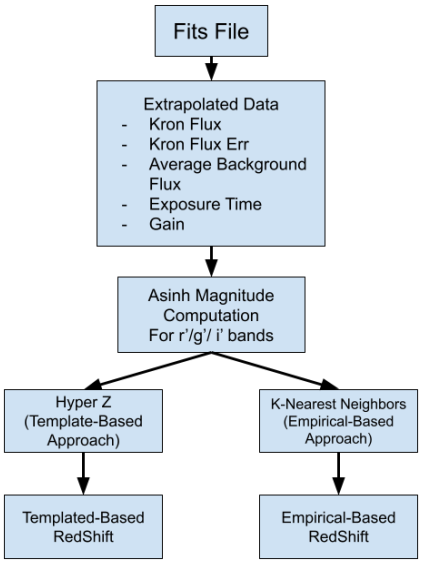

FIG. 2: A basic schematic outlining the experimental procedure.

A. Observational Methods

As mentioned previously, the LCO telescope we used is the 0.4 meter SBIG STL-6303. The telescope has SDSS u',g',r', and i' filters. Each individual filter covers a section of the visible light spectrum and only lets in light within their range. The wavelength range for each filter is depicted in Figure 3.

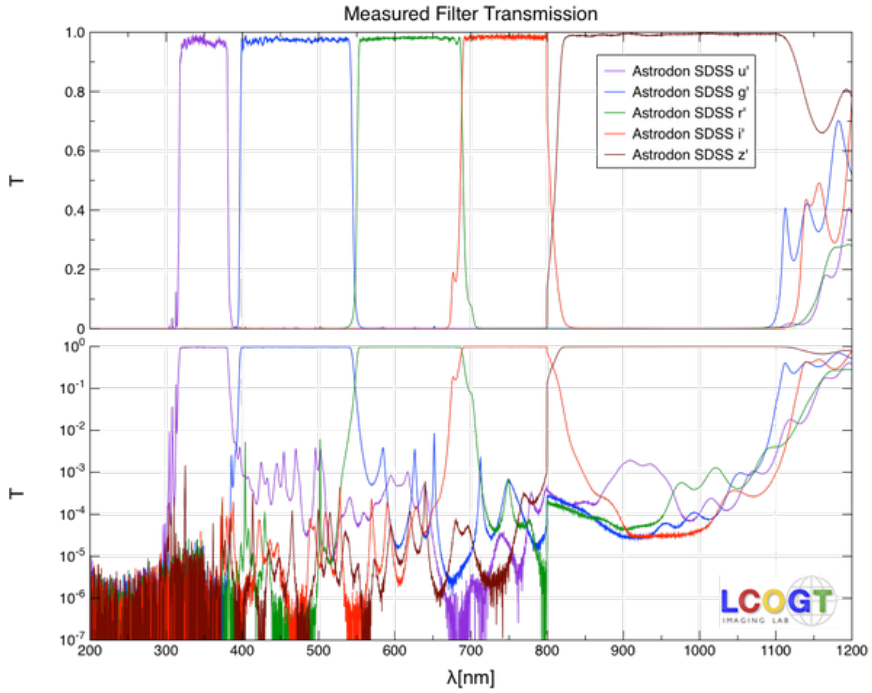

FIG. 3: A basic schematic outlining the experimental procedure. [8]

The LCO telescope system requires seven different input specifics to capture an image: target name, right ascension (RA), declination (DEC), filter type, number of exposures, exposure time, and observational windows. Right ascension and declination are the equatorial coordinate system that locates the target object. The number of exposures is how many images are captured for each filter, and the exposure time is how long the aperture of the telescope will be open for each filter.

The telescope observations requested specifics for Galaxies A to D are displayed in Table II. Galaxy A is the Sombrero Galaxy, known to have a lower redshift and higher magnitude. Its high magnitude allows for exposures using the u' filter and for less exposures taken. Galaxies B, C, and D have higher redshift, are farther away, and harder to detect. The telescopes detect few photons from these galaxies in the u' filter and they cannot be differentiated from the background noise. As a result, the u' filter is ignored and more exposures are taken to increase the photon count.

Images retrieved from the LCO telescope undergo a pre-processing system called the

Galaxy	RA (HH:MM:SS)	Dec(HH:MM:SS)	SDSS Filters	Exposures per Filter	Exposure Time (s)
A_{exp}	$+12:39:59.43$	$-11:37:22.97$	u',g',r',i'	5	100
B_{exp}	$+12:27:52.30$	$-11:20:37.1$	g',r',i'	10	100
C_{exp}	$+12:46:20.79$	$-42:41:38.0$	g',r',i'	10	100
D_{exp}	$+12:58:22.25$	$-03:06:05.7$	g',r',i'	10	100

TABLE II: Observational methods. This table displays the coordinates where the telescope was aimed towards for each galaxy and which filters were used to capture the galaxy.

Beautiful Algorithms to Normalize Zillions of Astronomical Images (BANZAI) pipeline. This algorithm removes noises, dead pixels, telescope biases, and corrects flaws. There are four main BANZAI processes: bad-pixel masking, bias subtraction, dark subtraction, and flat-field correction. The following paragraph summarizes the function of each of the processes.

The bad-pixel masking removes or masks dead pixels, pixels that cannot absorb light, in the photon detectors of the telescope. These dead pixels may arise from damage to or overuse of a telescope. Bias subtraction removes the readout noise of a telescope when capturing an image. This is the extra noise that the telescope detects when the aperture is covered. Dark subtraction removes any noise that is caused by heat generated by the telescope during long exposures. Flat field correction cleans up any deformities caused by the telescope lens, such as image darkening or disfigurement [9].

The BANZAI processed images then undergo a Source Extraction Process (SEP), which attaches information and data to the image, such as the location, filter type, gain or the air mass and wind speed when the exposure was taken. Each data type is called a header. The resulting image and data file is a fits file [10]. Finally, the astrometric calibration program which attaches the equatorial coordinates to each fits file [11]. The final fits file is retrieved by us to analyze.

B. Data Extrapolation

Using astropy and other basic python libraries, we extrapolated the necessary data from the fits files. Five pieces of data are needed for each fit file: the gain of the telescope, the exposure time, the peak flux value of the targeted object, the error on the flux peak value of the targeted object, and the average background flux value at the targeted object. All fluxes in the FITS files are displayed in counts. The code extrapolates the required data from the headers of each fits file.

The flux values extracted from the fits file are called kron flux values. These are flux values measured with the aperture within the kron aperture radius. Over 90% of the celestial object's flux is captured within the kron radius [12]. In this experiment, the kron peak flux is chosen over all other given flux values to ensure that the majority of the photons from the galaxy have been recorded.

To calculate the magnitude of the galaxy, the flux per each filter must be in joules per second. Let f be the index for the filter type (g',r',i') and let i be the index for each fit file with filter f. The equation to calculate the flux in joules per second is as follows:

$$F_f = \frac{\sum_i K_i \times G_i}{\sum_i t_i} \times (1.602 \cdot 10^{-19} J) \tag{2}$$

Where K_i is the kron peak flux in counts, G_i is the gain (electrons per count), and t_i is the exposure time. By summing the total electrons and the total exposure time for each fit file and dividing the two sums, we calculate our flux value in joules per second. This flux calculation process is repeated for each filter of each galaxy.

C. Asinh Magnitudes

As previously mentioned, this experiment utilizes asinh magnitudes. This system was created to take account the differences between the accepted and experimental magnitudes

recorded through the SDSS filters [13]. The asinh scale improves the accuracy of fainter objects [6]. The formula to calculate asinh magnitude is as follows:

$$m = -\frac{2.5}{\ln(10)}\left[\text{asinh}\left(\frac{(f/f_0)}{(2b)}\right) + ln(b)\right] \tag{3}$$

Where f is the flux density of the source, f_0 is the 0 flux density through the filter, and b is the softening parameter. The values for f_0 and b vary upon filters. The softening parameter values are depicted in Table III. The softening parameter is found by setting it to a single standard deviation of the sky noise [**?**]. The f_0 value ends up being 3631 jansky. The flux density values are in units of janskies , where the conversion is $10^-26W * m^{-2}Hz^{-1}$ per jansky. The asinh magnitude error is calculated by equation 4, where err is the flux error in counts and t is the exposure time.

$$m_{error} = \frac{2.5}{\ln(10)}\frac{err}{t \cdot 2b}(\frac{f}{f_0})\sqrt{1 + \frac{(f/f_0)}{2b}^2}^{-1} \tag{4}$$

Band	b	Zero-Flux Magnitude $[m(f/f_0 = 0)]$	$m(f/f_0 = 10b)$
u	1.4 $\times 10^-10$	24.63	22.12
g	0.9 $\times 10^-10$	25.11	22.60
r	1.2 $\times 10^-10$	24.80	22.29
i	1.8 $\times 10^-10$	24.36	21.85
z	7.4 $\times 10^-10$	22.83	20.32

TABLE III: This table, from the Sloan Digital Sky Survey: Early Data Release ([14]), shows the softening parameter, b, for each filter band, as well as the Zero-Flux magnitude, and the $f = f_0 10b$ magnitude value.

In order to use equation 3 and 4, the flux from equation 2 must be converted into janskys. This is done by dividing the flux by the area of the telescope and the bandwidth of each

filter. The bandwidth is determined by finding the frequency of the central wavelength of each filter from Figure 3.

The flux densities of all filters per galaxy are computed and plugged into equation 3 where $f_0 = 3631$ janskys.

Both template-based and empirical based approaches required AB magnitude scale inputs. This scale is defined using the following formula where f_{AB} is in janskys.

$$m_{AB} = -2.5 \log(\frac{f_{AB}}{3631 Jy}) \tag{5}$$

Note that the magnitude zero flux is 3631 Jy. The SDSS asinh magnitudes are meant to be on the same scale as the AB system, but slightly off [15]. For SDSS u and z band filters, there is a slight difference between AB and Asinh magnitudes up to a difference of 0.04 magnitude. The experimental telescope does not have a z band filter, and we purposely ignored the u band filter. Therefore, it is safe to conclude that experimental asinh magnitudes are equal to the AB magnitude [16].

D. Template-Based Approach: HyperZ

The template-based approach is conducted using a program called HyperZ, a coding package that estimates the redshift by Spectral Energy Distribution (SED) fitting. A basic schematic detailing the HyperZ process is displayed in Figure 4.

HyperZ estimates redshifts by taking an input of the photometric catalog containing their AB magnitudes and their error per filter. It takes the inputs and converts them into fluxes that can be dereddened. Dereddening removes the extra red color that a distant object may appear. In our experiment, dereddening was not computed on any magnitudes due to low redshift values. The program utilizes a hypercube, made from the inputted parameters, which helps select a SED template. These templates replicate the colors of the galaxies at different spectral types. Models are generated from Star Formation Rates (SFR). SFR are

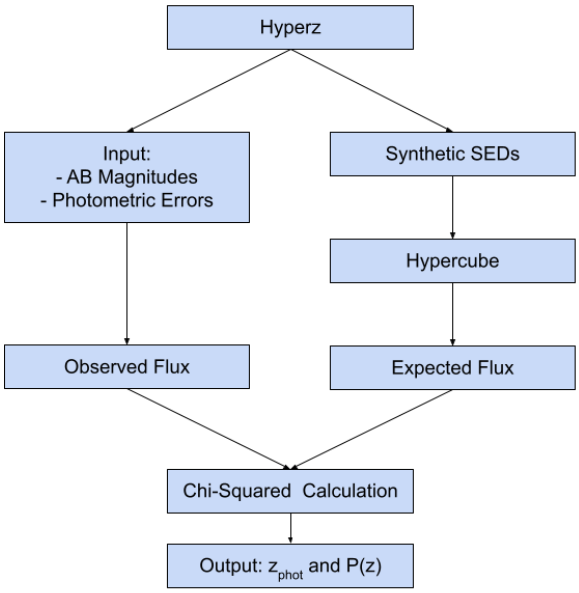

FIG. 4: A basic schematic outlining the HyperZ program.

determined by Schmidt's law, the SFR of a star is dependent on the power of the density of the interstellar gas. This model yields equation

$$\psi(t) \propto e^{-t/\tau} \tag{6}$$

Where τ is the timescale and n is the power of the interstellar gas density. There are five different SED: one of a single burst of SFR, one with a timescale of 1 Gyr, one with timescale 3 Gyr, one with timescale 15 Gyr, and one with constant SFR. The different timescales represent different galaxies such as young, spiral, and irregular galaxies. The lyman forest is applied onto the spectra. This is due to the fact that galaxies of higher redshift loses their flux as it penetrates through the Earth's clouds.

Afterwards, the hypercube generates expected fluxes for the SED by using the SDSS filter response functions. Finally, the program outputs redshifts with the lowest difference between experimental flux and calculated flux using chi square formula below:

$$\chi^2(z) = \sum_{i=1}^{N_{Filters}} \left[\frac{F_{obs,i} - b \times F_{Temp,i}(z)}{\sigma_i} \right]^2 \tag{7}$$

Where $F_{obs,i}$ is the experimental flux from the observed SED, $F_{Temp,i}$ is the calculated flux from the template, σ_i is their uncertainty in filter i, and b is a normalization constant.[17]

E. Empirical-Based Approach: K-Nearest Neighbors

The empirical-based approach is conducted using the k-Nearest Neighbor Algorithm and around 177,300 different celestial objects from the SDSS DR 17 database [5]. In short, the code estimates a data point value based on the known k amount of neighbors of similar values. Let i be an index for our experimental galaxies in the query set and let j be an index for objects in the training set. Our experimental code attempts to minimize the following equation:

$$z_{phot} = c_i + a_i d_i \tag{8}$$

Where z is the estimated photometric redshift, c is an offset term, $d_i is a parameter vector value, and a is the coefficient vector for d. This uses Becket al. (2016) and Taunket al. r magnitude, g-r color index, and r-i color index. Color indices are the difference between two different filt$

The nearest neighbors to the imputed galaxies are determined by minimizing the chi-square equation [18]:

$$\chi^2(z) = \sum_{j \in NN} \frac{(z_j - c_i - a_i d_j)^2}{w_j} \tag{9}$$

However, due to the difficult minimization method, our experiment utilizes a personal and more simple distance metric.

$$D = \sum_{j \in NN} |d_i - d_j| = \sum_{j \in NN} (r_i + g - r_i + r - i_i) - (r_j + g - r_j + r - i_j) \tag{10}$$

The distance metric describes how different the training data is from the query data. The code calculates the distance metric between the inquiry galaxy and all objects in the training set. We set $k = 100$. This means the top 100 objects with the smallest distance metric is used to compute the predicted redshift value. Let NN be an index for all k objects that have the smallest distance metric. The predicted redshift is calculated as the average of all known redshifts in k:

$$z_{predicted} = \sqrt{\frac{\sum_{j \in NN} z_j}{k}} \tag{11}$$

And the error is given by the following

$$\delta z_{phot,i} \approx \sqrt{\frac{\sum_{j \in NN} (z_j - z_{predicted})^2}{k}} \tag{12}$$

III. RESULTS

To mention once again, all the galaxies are labeled following the reference chart in Table I. Galaxies A - D are captured on the LCO telescope and are our experimental galaxies. Galaxies E and F are test galaxies whose accepted values are found on Simbad [7].

A table of all the resulting r', g', and i' band magnitudes and their errors for each galaxy are shown in Table IV using equations 3 and 4.

A. Template-Based Results

By taking all the values in Table IV and computing the SEDs in HyperZ, we obtain the template-based redshifts displayed in Table V and the empirical-based redshifts displayed in Table VI.

HyperZ does not provide a specific error value. Instead, HyperZ outputs a probability percentage that the predicted redshift value is correct. From the manual, the program

	r' magnitude	r' error	g' magnitude	g' error	i' magnitude	i' error
A_{exp}	13.47746163	75.87	14.79941838	53.91	13.56564163	58.78
B_{exp}	20.5571003	2.68	21.70406992	2.22	20.96777631	2.41
C_{exp}	20.41815517	2.56	22.09272542	1.59	20.55157546	2.51
D_{exp}	19.38510287	3.44	20.70239522	3.02	19.61346501	3.05
D_{acc}	17.511	0.007	18.441	0.01	17.051	0.007
E_{acc}	11.529	0.002	12.219	0.002	11.237	0.002
F_{acc}	11.613	0.006	12.284	0.006	11.081	0.007

TABLE IV: This table contains all the asinh magnitudes and their errors for all galaxies using equation 3 and 4. The magnitudes listed in the last three rows are AB magnitudes from SIMBAD or SDS [7].

Galaxy	Accepted Redshift	Hyperz Redshift	Probability (%)	Percent Error
A_{exp}	0.00342 ± 0.00002	0.443	100.00	12900%
B_{exp}	0.0850 ± 0.0002	0.385	99.40	353%
C_{exp}	0.0477 ± 0.0002	0.430	99.33	801%
D_{exp}	0.113 ± 0.00003	0.423	99.81	274%
D_{acc}	0.113 ± 0.00003	0.065	97.63	42.5%
E_{acc}	0.000811 ± 0.000016	0.066	97.58	8038%
F_{acc}	0.00326 ± 0.00007	0.607	96.53	18500%

TABLE V: This table displays estimated redshifts using the Hyperz method. The values are calculated using values in Table IV

struggles to predict redshifts under a redshift 0.05 and has a higher chance of predicting incorrect redshifts. This illustrates that lower redshift galaxies will have difficulty to receive a correct photometric redshift estimate. This is most likely due to the fact that the model

spectral templates given by HyperZ ranges across higher redshift values. Most predicted redshift values have a percent error over 100%. Therefore, a template-based approach is not the best method to predict redshifts using photometric surveys specifically for smaller diameter telescopes.

Galaxy	Accepted Redshift	Nearest Neighbors Redshift	Percent Error
A_{exp}	0.00342 ± 0.00002	0.326 ± 0.449	9430%
B_{exp}	0.0850 ± 0.0002	0.458 ± 0.269	439%
C_{exp}	0.0477 ± 0.0002	0.420 ± 0.205	781%
D_{exp}	0.113 ± 0.00003	0.310 ± 0.105	174%
D_{acc}	0.113 ± 0.00003	0.125 ± 0.122	10.6%
E_{acc}	0.000811 ± 0.000016	0.000461 ± 0.000000	43.2%
F_{acc}	0.00326 ± 0.00007	0.000461 ± 0.000000	85.9%

TABLE VI: This table displays estimated redshifts using the K-Nearest Neighbor method. The values are calculated using values in Table IV

In contrast to HyperZ, the k-Nearest Neighbors method displays more promising results. The redshift and its error was calculated using equation 11 and 12. For galaxies A through C, this method predicted redshifts with high precision. When decreasing in redshifts, the percent error exponentially increases. The statistical error that could play into this huge error starts with the training set. While there are about 177,302 different celestial objects in the data sets with varying redshifts. There are only around a thousand or less of those celestial objects with redshift less than one. As a result, there is not enough variety of objects in the SDSS DR 17 that has accepted redshift values lower than 0.1. Percentage error decreases at higher redshift above 0.1. This can be seen on the D_{acc} row in Table VI which uses the accepted values from the same galaxy as D_{exp}. Rows E_{acc} and F_{acc} also displayed low percent error. The lower percent error from all accept values indicates two

possibilities. One, the experimental magnitude values are vastly incorrect, which caused the experimental values to have higher error. Two, the training set is too small and requires more data with varying redshifts amongst all magnitudes. The magnitude values in Table IV are above 10 magnitude in error. This could arrive from incorrect magnitude formulas or poor conversion of values. The huge magnitude error could also stem from a variety of systematic errors.

Both methods are affected by fourth sources of systematic error: background flux, reddening, magnitude conversion, and quantum efficiency. We try to take into account the background flux by removing the flux before the magnitude calculation. We did not take into account any sources of reddening due to the fact that the accepted redshifts are low enough to not be affected. As previously mentioned, the conversion from asinh to ab magnitude scale is practically equivalent with a 0.02 to 0.04 magnitude difference in the u and z bands [15]. However it is possible that there is a slight difference between the scales at g, r, and i filters. Quantum efficiency is the measure of the effectiveness of the detector. In this experiment, we did not take into account the quantum efficiency of the SBIG STL-6303 telescope. This can cause a shift in the amount of flux coming into our telescope that is truly detected by telescope. Other systematic errors is accounting for air mass, wind speed, weather, and atmosphere conditions that could have potentially prevented photons from entering the detector.

All in all, the results could possible indicate that photometric redshift calculation using small telescopes

IV. DISCUSSION

We have obtained reasonable asinh magnitude values in IV. In contrast, the error magnitude is highly unreasonable and not precise indicating that the flux conversion into asinh magnitude values is incorrect. We cannot comment on the precision of the template-based

method, as it does not provide a clear uncertainty for its predicted redshift values. There are no experimental redshift values that have the accepted value lie within its range of uncertainty, showing that our measurements are heavily inaccurate. Both methods yielded high percent error which is indicative that major experimental improvements must be made.

Several improvements that can be made is to account for the rest of the systematic errors listed in the results section: reddening, magnitude conversion, and quantum efficiency. The amount of flux being detected by our telescope is key to accurate magnitude calculation. While the experimental galaxies' redshifts may be low, de-reddening the flux values may improve magnitude calculation. By applying correct Asinh to AB magnitude conversion and accounting for quantum efficiency. To see if our methods worked at higher redshifts, we could possibility test our methods using experimental data from higher aperture telescopes. In addition, both template and empirical methods used three input dimensions to estimate a redshift value. By including more dimensions by collecting data in the u and z band, we can improve the accuracy of our values. Last but not least, specifically for the empirical method, a new training set is necessary. The current training set obtained from SDSS DR17 do not have variety within their lower end redshfit values. We could further improve the empirical method by obtaining data elsewhere.

Photometric redshift estimation is a difficult process to calculate, especially using smaller aperture telescopes. There are many complex variables and factors that can fluctuate the accuracy of our calculation values. In the end, photometric redshift is still significant in mass-producing redshift estimates for many database. Further investments in the field can lead towards bigger goals in astrophysics.

V. REFERENCES

[1] Pierre Lena, Daniel Rouan, Francois Lebrun, Francois Mignard, and Didier Pelat. *Observational Astrophysics.* Springer, 3 edition, 2008.

[2] NASA.

[3] L. Casagrande and Don A. VandenBerg. Synthetic stellar photometry – i. general considerations and new transformations for broad-band systems. *Monthly Notices of the Royal Astronomical Society*, 444(1):392–419, August 2014. doi: 10.1093/mnras/stu1476. URL https://doi.org/10.1093/mnras/stu1476.

[4] Kashvi Taunk, Sanjukta De, Srishti Verma, and Aleena Swetapadma. A brief review of nearest neighbor algorithm for learning and classification. In *2019 International Conference on Intelligent Computing and Control Systems (ICCS)*. IEEE, May 2019. doi: 10.1109/iccs45141.2019.9065747. URL https://doi.org/10.1109/iccs45141.2019.9065747.

[5] Katherine Accetta, Conny Aerts, Victor Silva Aguirre, Romina Ahumada, Nikhil Ajgaonkar, N Filiz Ak, Shadab Alam, Carlos Allende Prieto, Andres Almeida, Friedrich Anders, et al. The seventeenth data release of the sloan digital sky surveys: Complete release of manga, mastar, and apogee-2 data. *The Astrophysical Journal Supplement Series*, 259(2):35, 2022.

[6] Robert H. Lupton, James E. Gunn, and Alexander S. Szalay. A Modified Magnitude System that Produces Well-Behaved Magnitudes, Colors, and Errors Even for Low Signal-to-Noise Ratio Measurements. *The Astronomical Journal*, 118(3):1406–1410, September 1999. doi: 10.1086/301004.

[7] M. Wenger, F. Ochsenbein, D. Egret, P. Dubois, F. Bonnarel, et al. The SIMBAD astronomical database. The CDS reference database for astronomical objects. , 143:9–22, April 2000. doi: 10.1051/aas:2000332.

[8] Las Cumbres Observatory. Transmission functions. URL https://lco.global/observatory/instruments/filters/.

[9] Curtis McCully, Monica Turner, N Volgenau, Daniel Harbeck, et al. Lcogt/banzai: Initial release (0.9.4). 2018. doi: 10.5281/zenodo.1257560. URL https://doi.org/10.5281/zenodo.1257560.

[10] E. Bertin and S. Arnouts. SExtractor: Software for source extraction. *Astronomy and Astro-*

physics Supplement, 117:393–404, June 1996. doi: 10.1051/aas:1996164.

[11] Dustin Lang, David W. Hogg, Keir Mierle, Michael Blanton, and Sam Roweis. Astrometry.net: Blind astrometric calibration of arbitrary astronomical images. *The Astronomical Journal*, 139 (5):1782–1800, March 2010. doi: 10.1088/0004-6256/139/5/1782.

[12] R. G. Kron. *Photometry of a Complete Sample of Faint Galaxies.* PhD thesis, University of California, Berkeley, December 1978.

[13] Chris Stoughton and Robert H. Lupton et al. Sloan digital sky survey: Early data release. *The Astronomical Journal*, 123(1):485–548, January 2002. doi: 10.1086/324741. URL `https://doi.org/10.1086/324741`.

[14] Chris Stoughton, Robert H. Lupton, Mariangela Bernardi, Michael R. Blanton, Scott Burles, et al. Sloan Digital Sky Survey: Early Data Release. *The Astronomical Journal*, 123(1):485–548, January 2002. doi: 10.1086/324741. URL `https://iopscience.iop.org/article/10.1086/324741/pdf`.

[15] J. B. Oke and J. E. Gunn. Secondary standard stars for absolute spectrophotometry. *The Astrophysical Journal*, 266:713, March 1983. doi: 10.1086/160817. URL `https://doi.org/10.1086/160817`.

[16] R. C. Bohlin, M. E. Dickinson, and D. Calzetti. Spectrophotometric standards from the far-ultraviolet to the near-infrared: STIS and NICMOS fluxes. *The Astronomical Journal*, 122(4): 2118–2128, October 2001. doi: 10.1086/323137. URL `https://doi.org/10.1086/323137`.

[17] Micol Bolzonella, Joan-Marc Miralles, and Roser Pell´o. *HyperZ v1.2 User's Manual*, 1999. URL `http://www.bo.astro.it/~micol/Hyperz/hyperz_manual1.2.pdf`.

[18] Róbert Beck, László Dobos, Tamás Budavári, et al. Photometric redshifts for the SDSS Data Release 12. *Monthly Notices of the Royal Astronomical Society*, 460(2):1371–1381, 04 2016. ISSN 0035-8711. doi: 10.1093/mnras/stw1009. URL `https://doi.org/10.1093/mnras/stw1009`.